Journal of Catalysis **198,** 243–255 (2001)
doi:10.1006/jcat.2000.3129, available online at http://www.idealibrary.com on IDEAL®

Pd–Mn Silica-Supported Catalysts

2. Description of the Catalytic Sites and Surface Properties for CO and NO Chemisorption

A. J. Renouprez,[1] J. F. Trillat, G. Bergeret, P. Delichère, J. L. Rousset, J. Massardier, D. Loffreda, D. Simon, F. Delbecq, and P. Sautet

Institut de Recherches sur la Catalyse, CNRS, 2 Avenue A. Einstein, F69626, Villeurbanne Cedex, France

Received July 14, 2000; revised November 28, 2000; accepted November 29, 2000; published online February 8, 2001

To explain the beneficial effect of Mn addition to Pd catalysts in CO–NO conversion, a detailed study of the surface structure and composition of the catalytic sites was undertaken. The combination of analytical microscopy and EXAFS confirms the presence of bimetallic particles in which manganese is partly alloyed to palladium, as described in Part 1 (A. J. Renouprez, J. F. Trillat, B. Moraweck, J. Massardier, and G. Bergeret, *J. Catal.* **179, 390 (1998)). Monte-Carlo modeling coupled with a simple energetic model and low-energy ion scattering (LEIS) shows that Mn has a larger concentration at the surface of the particles than the mean value measured by chemical analysis. This is attributed to a segregation of this element at the surface. To establish a correlation between the structure of these particles and their reactivity, infrared experiments of CO, NO adsorptions and coadsorption were carried out at both 300 and 573 K. The measured frequencies were interpreted on the basis of density functional theory (DFT) quantum chemical calculations. At 300 K, on pure Pd, CO and NO are located on the same sites and are displaced by each other. On the alloys, both molecules remain partly on the surface on adsorption of the other. DFT calculations show that the Mn atom at the surface induces a significant shift of the NO stretch frequency to lower values, especially if a Mn atom is present in the surface site. On mixed Pd–Mn sites, the chemisorbed NO molecule is found in a geometry quasi-parallel to the surface, with a long N–O bond and a low stretch frequency. This structure is stable on Pd_3Mn, but not on pure Pd. This lying down geometry is a precursor for the dissociation. A dual-functional mechanism for the NO reduction, involving Mn oxides with oxygen vacancies and this form of adsorbed NO, is proposed.**

Key Words: **palladium–manganese; bimetallic catalysts; Pd–Mn alloy; CO–NO infrared spectroscopy; electronic structure modifications; density functional theory calculations.**

1. INTRODUCTION

The reduction of NO emission by diesel engines down to 10 g/kg of consumed fuel is an ambitious target (1) which will be the legislative standard in Europe as soon as 2005. With this objective, it is necessary to improve simultaneously many technological elements. Among them, air–fuel mixing, rate of injection, compression ratio, filtering of particles, and catalysts for the treatment of exhaust gases all have to be improved. When only NO abatement is required in the exhaust gases, in the presence of oxygen and hydrocarbons, it has been shown for example that copper on ZSM-5 appears to be one of the most active catalysts (2). Actually, many recent studies have shown that zeolite–supported metals are reasonably efficient (3).

If both CO and NO have to be eliminated, one uses at present catalysts essentially based on platinum and palladium associated with rhodium or/and cerium (4). For the design of new and cheaper catalysts for this treatment of exhaust gases, one of the main difficulties is the reduction of the light-off temperature, to obtain reasonable efficiency when the engine has not yet reached its working temperature.

An alternative way of using an association of noble metals would be to incorporate into palladium cheaper metals like those in the fourth row of the Periodic Table. This was successfully achieved with Pd promoted by cobalt oxide (5) or, as we have shown recently, with Pd–Mn (6) and Pd–Cr couples (7), which lower the light-off temperature of conversion by 80 to 100 K, compared with pure palladium. The effect observed with Pd–Mn, illustrated in Fig. 1, has been tentatively attributed to improved activation of the NO molecule. The present work aims to explain this synergetic effect by infrared spectroscopy experiments of CO and NO adsorption, interpreted with the help of quantum chemistry calculations.

In a preceding paper (8) the preparation of Pd–Mn silica-supported catalysts obtained by the decomposition of acetylacetonate precursors was described. Analytical microscopy (EDX) and EXAFS demonstrated that part of the manganese is dispersed on the support in the form of oxide, MnO_x, but also that bimetallic Pd–Mn particles are formed in which part of the manganese is alloyed to palladium. This characterization is completed here by a

[1] To whom correspondence should be addressed. E-mail: renoupre@catalyse.univ-lyon1.fr.

0021-9517/01 $35.00

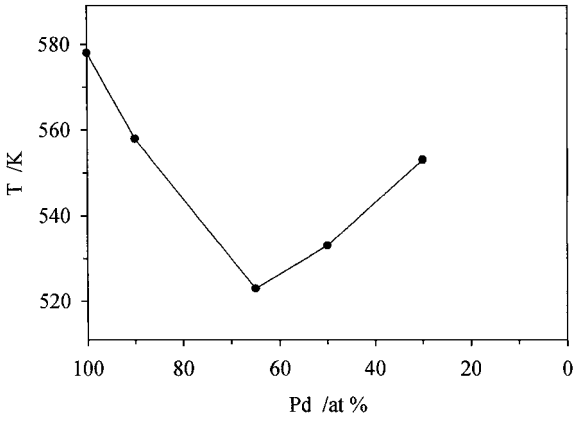

FIG. 1. Dependence on the Pd–Mn composition of the light-off temperature of NO in CO–NO conversion. Reprinted, with permission, from Trillat *et al.* (6).

low-energy ion scattering (LEIS) study, providing the details on surface structure and composition (Table 1).

2. EXPERIMENTAL AND THEORETICAL METHODS

2.1. Low-Energy Ion Scattering and XPS

To determine the surface composition of the catalysts, it has been established that LEIS is to be preferred to XPS (9, 10), because it yields the composition of the surface layer only. Indeed, the photoelectrons produced in XPS have a mean free path on the order of 1.5 to 3 nm and consequently probe several layers. Concerning LEIS, the survival probability of ionized states is on the order of 1–2% for collisions involving the first atomic layer and is effectively zero for ions that penetrate below the first layer. LEIS experiments were performed with 1-keV ^{4}He ions in an ESCALAB 200R from VG Scientific. A treatment chamber connected to the spectrometer allows the activation of catalysts in hydrogen up to 800 K.

Quantitative analysis of the surface composition must take into account the cross sections of the various surface atoms. The concentration ratio can be expressed with respect to the areas A of the peaks located at about 768 and 875 eV corresponding, respectively, to Mn and Pd:

$$\frac{C_{\mathrm{Mn}}}{C_{\mathrm{Pd}}} = \frac{A_{\mathrm{Mn}}}{A_{\mathrm{Pd}}} \times \frac{S_{\mathrm{Pd}}}{S_{\mathrm{Mn}}}. \qquad [1]$$

The S_{Pd} sensitivity has been measured by calibration with a Pd(100) single-crystal face, but a Mn single crystal was not available. Thus, we used polycrystalline Mn flakes (99.98% purity) from Goodfellow to determine a sensitivity factor, S_{Mn}. A carefully polished Mn flake was submitted to several ion bombardments and annealing treatments. No impurities were detected in the spectrum, excepted oxygen, a contaminant that could never be totally eliminated. Assuming a bcc unit cell, which is the stable phase below 1000 K, one obtains an atomic density of 1.33 10^{15} at./cm^2, if (111), (100), and (110) planes are equally distributed at the surface. The ratio of the S factors turns out to be 2.8. It can be compared with the values previously measured for Pd–(Cu, Ni, Fe) pairs (10, 11), respectively, found to be equal to 2.2, 2.3, and 2.4. In the present case, because of the presence of oxygen, which reduces the Mn signal, the uncertainty with respect to the S ratio can be on the order of 20 to 30%. Additionally, the Mn signal is strongly dependent on the unknown surface roughness of the flake, increased by the ion bombardments.

To avoid the possible sputtering of the atoms of the first layer by He ions during measurement, the beam flux was set at a low value, 40 nA/mm^2, which is sufficient to obtain good statistics ($N^{1/2}/N \approx 10\%$) within 30 s. The ion dose to which the sample is submitted during one acquisition is thus 1.25×10^{15} ions/cm^2. Assuming a sputtering yield on the order of 0.1 for He, one can admit that only 0.10–0.15 ML is sputtered during the first spectrum which reflects the composition of the outermost layer. On the other hand, one can also take advantage of the sputtering to obtain information on the composition of underlying layers by increasing the time of measurement. Twenty successive scans were thus performed, separated by 1 min of sputtering each time.

XPS experiments were also performed on the same instrument using an Al X-ray source and a hemispheric analyzer. The internal reference for the binding energies is the Si 2*p* level located at 103.4 eV (12).

TABLE 1

EM, EDX, EXAFS, and LEIS Results and Predictions on Individual Bimetallic Particles

Sample	EM (d_s, nm)	EDX (Pd, at.%)	EXAFS (Pd, at.%)	LEIS[a] (surface Pd, at.%) A	LEIS[a] (surface Pd, at.%) B	Predictions[b] (surface Pd, at. %)
$Pd_{90}Mn_{10}$	5	95	98	72	85–90	86
$Pd_{65}Mn_{35}$	4.9	75	87	37	62	52

[a] A and B are the concentrations measured respectively after 2 and 20 min of sputtering.

[b] On the basis of the atomic concentrations measured by EDX.

2.2. Infrared Spectroscopy

Infrared experiments of CO and NO chemisorption on bimetallic catalysts were carried out with a Bruker IFS 110 FTIR spectrometer. The 20-mm wafers (15–20 mg of catalyst) pressed at 2.5×10^5 kPa are placed in a quartz cell closed with CaF_2 windows. They are activated under hydrogen at the same temperature as during the preparation and evacuated at 573 K, and after adsorption of the reactants, the gas phase is removed by evacuation at the required

temperature. Spectra of the adsorbed species are obtained after subtraction of the contribution of the bare catalyst. Assignment of stretching frequencies to the adsorption modes is usually based on reference frequencies of molecular complexes. However, our recent frequency calculations of CO or NO on Pd(111) (13, 14) have shown that such an approach can lead to incorrect assignments and that density functional theory calculations yield very good agreement with experimental data. Therefore in the present paper the interpretation of IR spectra is based on quantum chemical calculations.

2.3. Quantum Chemical Calculations

The stable adsorption sites and the molecular stretch frequencies were calculated in the framework of density functional theory (DFT). The Vienna Ab initio Simulation Program (VASP) (15) was used with the exchange-correlation functional proposed by Perdrew *et al.* (16). This code develops the wavefunction of periodic systems on the basis of plane waves, with ultrasoft pseudopotentials to describe the atomic cores. The surface was modeled by a slab consisting of four metal layers. A 2×2 unit cell was used in the plane parallel to the surface, with NO or CO adsorption on one side of this slab. The chemisorption structures were fully optimized including surface relaxation in the first two layers, and the vibrational analysis was performed from a numerical calculation of the second derivatives of the energy. The degrees of freedom for this calculation involve the vertical displacement of the adsorbate atoms, the NO bonds being stretched, keeping the center of mass of the molecules fixed. Approximate anharmonic corrections were obtained from a more precise description of the potential energy surface for the deformation associated with each given eigenmode. In this estimation, the center of mass is kept fixed, the anharmonic coupling between eigenmodes being neglected.

3. RESULTS

3.1. Low-Energy Ion Scattering

The catalysts were submitted to calcination and reduction treatment during preparation (8), but as they were kept in air for several weeks, they have to be rereduced. They were thus introduced into the preparation chamber connected to the LEIS-XPS instrument and heated at 773 K under hydrogen (101 kPa) for 4 h, before evacuation at room temperature.

In Fig. 2 are shown the LEIS spectra of $Pd_{90}Mn_{10}$ and $Pd_{65}Mn_{35}$ samples recorded after 0.5, 6, and 12 min of sputtering. At the beginning of the analysis a concomitant decrease in the Mn signal and an increase in the Pd signal are observed. The variation in Pd surface concentration as a function of etching time, calculated from Eq. [1], is represented in Fig. 3 for the $Pd_{65}Mn_{35}$ sample, taking into account a ratio of the sensitivity factors of 2.8 between the two elements. It is known that rearrangements can occur under the effect of the ion beam, but because of the low flux, the first measurement gives some indication of the composition of the first layer. Moreover, Mn enrichment is certainly limited to the superficial layer, since after 5–6 min of sputtering, the concentration ratios remain nearly unchanged.

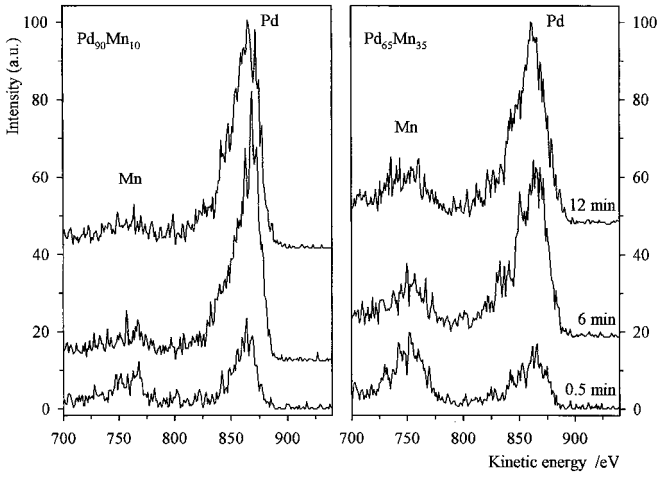

FIG. 2. LEIS spectra of $Pd_{90}Mn_{10}$ and $Pd_{65}Mn_{35}$ catalysts recorded after successive periods of sputtering.

To determine the contribution of the MnO located on the support to the overall Mn signal, a separate experiment was simultaneously carried out on $Pd_{65}Mn_{35}$ (containing 0.4 wt% Mn) and on pure Mn/SiO_2 (Mn concentration 3.2 wt%). Both samples were treated at 773 K in the preparation chamber and transferred to the spectrometer. The results presented in Fig. 4 compare the signals of Mn in MnO and in the $Pd_{65}Mn_{35}$ sample recorded after 0.5 min of sputtering. Taking into account the concentration ratios, one can conclude that the signal of Mn in MnO is approximately 20 times lower than in the bimetallic particles.

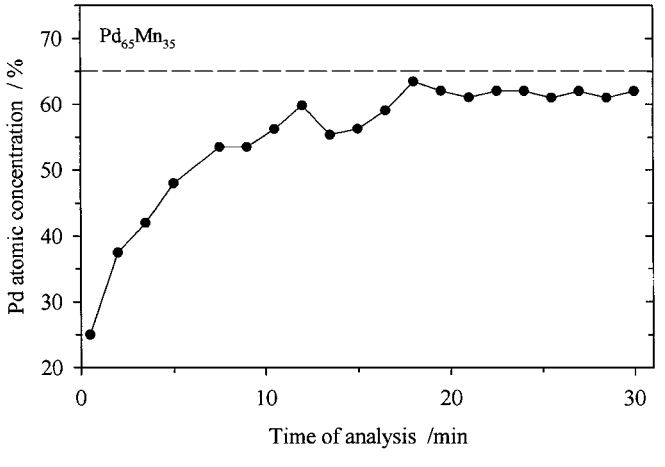

FIG. 3. Variation of the surface Pd concentration of the $Pd_{65}Mn_{35}$ catalyst with sputtering time.

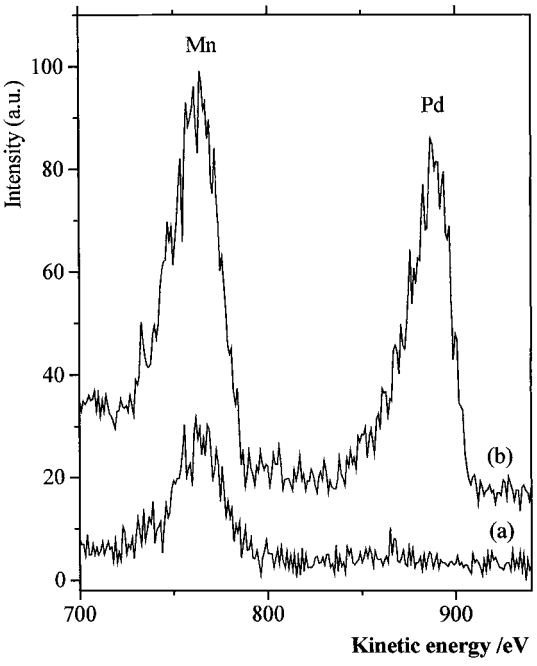

FIG. 4. Comparison of LEIS spectra of $Pd_{65}Mn_{35}$ (a) and 3.2 wt% Mn/SiO_2 (b) catalysts.

3.2. Infrared Study of CO and NO Chemisorption

3.2.1. CO and NO adsorption at 300 K. CO adsorption is carried out on the reduced-Pd supported clusters at 300 K, under 1.5 kPa, followed by an evacuation also at 300 K for 30 min. Under these conditions, which correspond to those used in metallic area determinations by chemisorption, the coverage is close to unity. The three usual infrared bands of adsorbed CO are observed on Fig. 5. Their assignment, discussed below, is given in Table 2. The highest band located

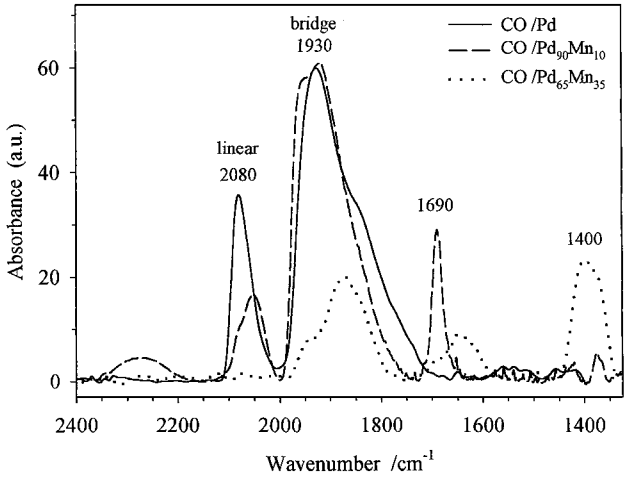

FIG. 5. Infrared spectra of CO adsorbed at 300 K on Pd (solid line) and on the two bimetallic catalysts $Pd_{90}Mn_{10}$ and $Pd_{65}Mn_{35}$ (dashed and dotted lines, respectively).

TABLE 2

Experimental and Calculated CO Stretching Frequencies on Pd Surfaces

	Pd/SiO_2		
Experimental	2080	1950	1850
Calculated	2085		1893
Assignment	On top	Bridge	Threefold

at 2080 cm^{-1} can be assigned to linear CO: on Pd(111) such top CO species were found to be stable in a high-coverage case (0.75 ML) from total energy calculations (14), with a frequency at 2085 cm^{-1}. These values are close to 2100 cm^{-1}, the value measured on (111) single-crystal faces (17). The second band is a broad peak near 1930 cm^{-1} (the same value on (111) single crystals). It can be tentatively decomposed into two subbands at 1950 and 1850 cm^{-1}. Their assignment is the subject of debate: the high-frequency mode is usually attributed to molecules in bridge sites, observed by LEED on (100) faces, and the lowest one to multibonded species.

From the calculation, it is found that threefold hollow sites with a stretch frequency of 1893 cm^{-1} coexist with the top site, at high coverage, on Pd(111). This is also a band observed on single-crystal faces (17). Our system cannot, however, be compared with a Pd(111) surface with 0.75-ML coverage, since, in that case, experiments show that the intensity for top sites is higher than that for hollow sites. Indeed, in these clusters of 2000–3000 atoms, formed of cubo-octahedra or truncated octahedra, the local structure is more comparable to that of stepped surfaces with an increased contribution of high coordination sites to the spectrum.

On the $Pd_{90}Mn_{10}$ bimetallic sample, the coverage measured by TDS is reduced to 0.75 ML. The intensity of the band corresponding to on-top CO species decreases and is shifted to 2050 cm^{-1} (Table 3). The bands assigned to CO adsorbed in bridge bonded and in threefold hollow sites undergo little modifications. But a new feature is observed at 1690 cm^{-1}, which can be assigned to CO molecules in high coordination sites containing a Mn atom. As will be shown later, in the case of NO, the presence of a Mn atom at the site strongly perturbates the molecule bonding, inducing a weakening of the stretch frequency. One should remark that this band is detected only when the sample has been equilibrated for 12 h at 773 K, so that mixed Pd–Mn layers can be formed at the surface, by segregation of Mn atoms.

On the $Pd_{65}Mn_{35}$ catalyst, the coverage is decreased to ≈0.25 ML. First, the on-top species is no longer observed, but a new feature appears at 1400 cm^{-1}. The broadband between 1800 and 2000 cm^{-1} has a shoulder at 1950 cm^{-1} which can be assigned to bridge sites, while the maximum of the peak at 1870 cm^{-1} would be associated with Pd_3 hollow sites. The band corresponding to mixed hollow sites is

TABLE 3

CO Adsorption on Pd–Mn Surfaces

	$Pd_{90}Mn_{10}$				$Pd_{65}Mn_{35}$			
Experiment	2050	1900	1850	1690	1950	1870	1650	1400
Assignment	On top	Bridge	Threefold	Fourfold	Bridge	Threefold	Fourfold	$Mn(CO_2)$

moved further down in frequency, to 1650 cm^{-1}. One should note that Blyholder and Allen (18) also observed bands at 1950 and 1890 cm^{-1} on pure manganese. An alternative possibility is to assign both the 1650 and 1400 cm^{-1} bands to a bicarbonate $Me(HCO_3)_2$ (ν_{as} and ν_s, respectively at 1615 and 1400 cm^{-1}) or to carboxylates, $Me(CO_2)$, with ν_{as} and ν_s at similar frequencies (19). This was indeed postulated by Srinivas *et al*. (20) in the case of CO adsorption on Au/TiO_2.

On NO adsorption on Pd/SiO_2, three infrared bands are observed (Fig. 6). The first two bands are rather sharp, at 1740 and 1640 cm^{-1}, while the third one is broad with several subbands ranging between 1500 and 1570 cm^{-1}. The results from the DFT calculations (14) show a strong influence of the NO binding site on frequency, with only little influence of the actual type of single-crystal surface, (111) or (100) (Table 4, Figs. 7 and 8). Complex variations of frequency appear as a function of coverage, but, from a compensation mechanism, the low- and high-coverage situations correspond to very similar frequencies. Let us, for example, consider the hollow site chemisorption on Pd(111). If one starts from the low-coverage situation ($\vartheta_{NO} = 0.33$ ML), the increase in coverage to 0.5 ML just leads to a higher ν_{NO} value, mainly from vibrational coupling between dipoles. However, on going to higher coverage ($\vartheta_{NO} = 0.75$ ML), the frequency decreases again because the electronic interaction with the surface is modified by the presence of top-site NO molecules on the unit cell (13).

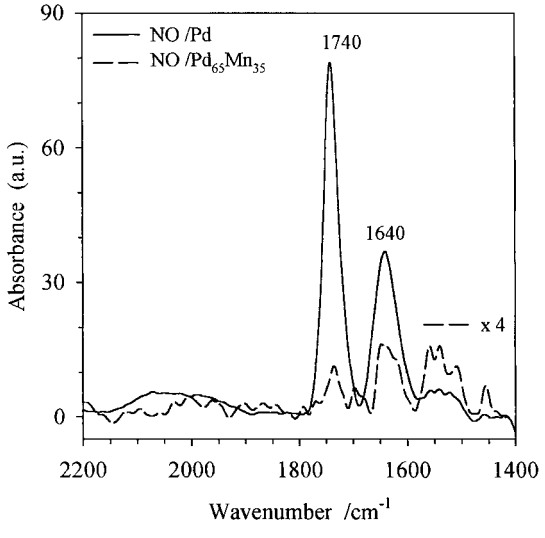

FIG. 6. Infrared spectra of NO adsorbed at 300 K on pure Pd (solid line) and on the $Pd_{65}Mn_{35}$ catalyst (dashed line; the absorbance is multiplied by 4).

All authors agree to assign the first band (1740 cm^{-1}) to linear species (21, 22). The frequency obtained from our DFT calculation for the top site on Pd(111), in the high-coverage structure, is slightly higher (1801 cm^{-1}, Table 4). This is, however, the closest possible assignment for this band from the calculations. This calculated value for the top site is only slightly modified in the case of low coverage on the (100) or (111) surface (1804 and 1812 cm^{-1}, respectively). The second band, at 1640 cm^{-1}, can to be assigned to bridge sites, most probably on (100) facets where such coordination is calculated to be stable with a calculated frequency of 1644 cm^{-1}. The third largest band is in the range of hollow sites. Such a hollow site can exist on a (100) surface: in fact the fourfold hollow site is not stable and distorts into a pseudo threefold one (Fig. 7c), the NO molecule interacting more strongly with three atoms of the surface (NO frequency 1500 cm^{-1}). It is also present on the (111) facets (frequency 1573 cm^{-1}) and these various possibilities (and others) for the hollow adsorption are certainly at the origin of the broadband. The assignments of the IR spectra are summarized in Table 4 and Fig. 8.

A significant change is observed in the IR spectrum in Fig. 6 when NO is adsorbed on the $Pd_{65}Mn_{35}$ alloy, with a strong general decrease in absorbance but a relative increase in intensity of the low-wavenumber bands. A new band is also present at low frequency. It is not possible from our calculations to interpret the absorbance change, and we therefore concentrate on the band assignment. A bulk-termination model is used for the (111) surface,

TABLE 4

Calculated and Experimental NO Stretching Frequencies on Pd Surfaces

Surface:	(100)			(111)			
Coverage:	0.25 ML			0.33 ML		0.75 ML	
Site:	Top	Bridge	Pseudo threefold	Top	Hollow	Top	Hollow
Label	a	b	c	d	e	f	f
ν (cm^{-1})	1804	1644	1500	1812	1574	1801	1573
Experimental ν (cm^{-1})			1740	1640	1570–1500		

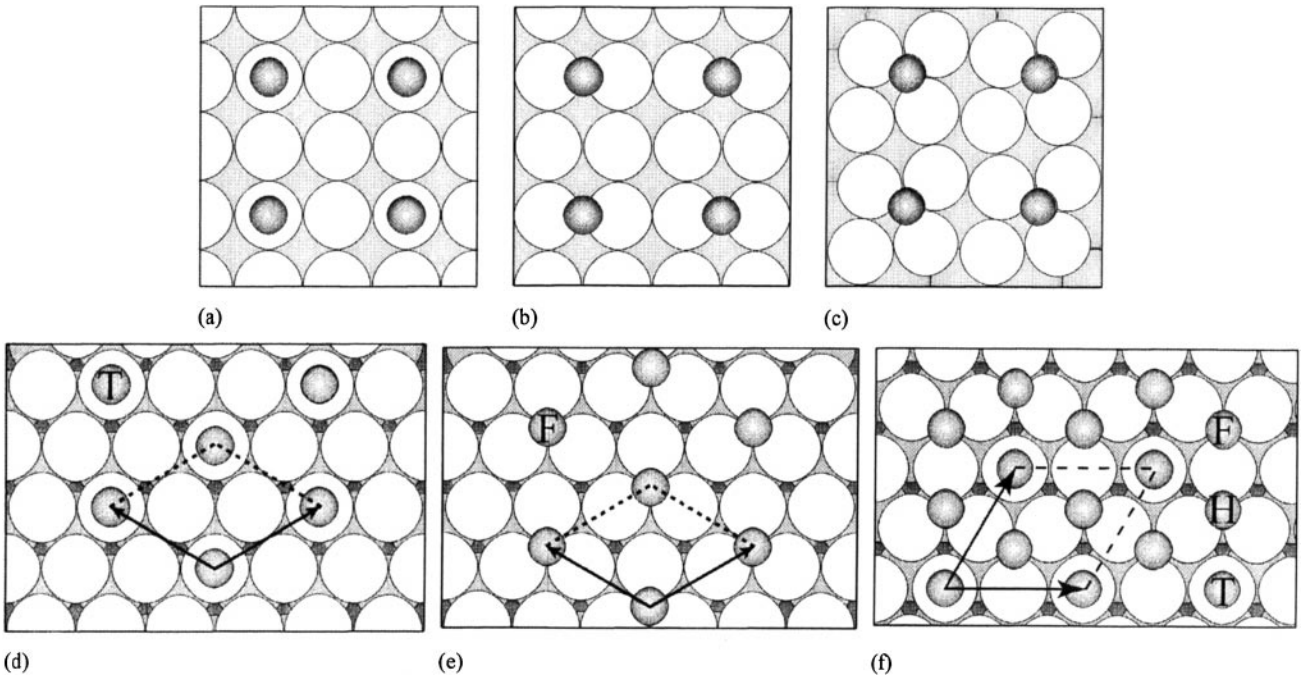

FIG. 7. Schematics of the structures considered for the calculation of the NO stretching frequency on Pd(100) and (111) surfaces. In these top views, the vertical NO molecule is seen as a single small dark ball, and the Pd atom as a large white ball. Labels are identical to those of Table 4: (a–c) top, bridge, and pseudo threefold sites at 0.25-ML coverage on Pd(100); (d–e) top and hollow sites at 0.33-ML coverage on Pd(111); (f) high-coverage structure (0.75 ML) on Pd(111) with a mixture of top and hollow sites.

resulting in a 2×2 unit cell with 1 Mn and 3 Pd atoms in the unit cell. Two terminations are possible for the (100) surface. The mixed surface, with equal amounts of Mn and Pd, was selected since its Pd–Mn stoichiometry is in better agreement with the Mn surface concentration found in the experiments.

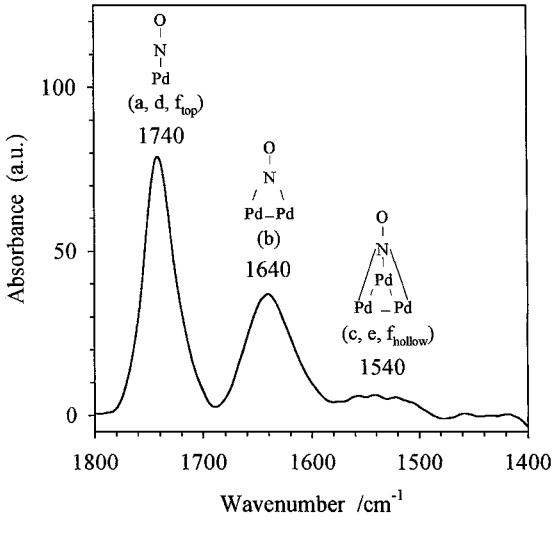

FIG. 8. Assignment of the IR bands of NO adsorbed on Pd from theoretical calculations.

Calculated frequencies at case $\frac{1}{4}$ ML on these model surfaces are listed in Table 5. The associated adsorption structures are depicted in Fig. 9, which shows the large variety of possible sites on (100) (A–F) or (111) (G–K) faces, while the frequency assignment is summarized in Fig. 10. A quick comparison of the experimental spectra for Pd and for the alloy suggests that, besides a change in intensity, the alloy shows only two new features at 1695 and 1455 cm^{-1}; the positions of the other bands apparently seem to be only slightly modified. The calculations indicate that such an analysis is incorrect and that even some of the peaks with unchanged frequency correspond to different NO binding sites on the alloy. The main general result is that, for a given site, the frequency is shifted to a lower value by $\approx$100 cm^{-1} if Mn atoms are involved in the chemisorption site. The top site on a Mn atom has good stability, and is associated with a NO stretching frequency of 1690 cm^{-1} on both model surfaces (Table 5). Hence the 1695 cm^{-1} peak can be assigned to that site. The situation is more complex for the top site on Pd. At low coverage the molecule adopts a tilted geometry (frequency 1684–1688 cm^{-1}) with an angle of 38° with respect to the normal to the surface. The upright geometry, however, is likely to be restored at high coverage, with a frequency of 1738 cm^{-1}, in good agreement with the 1730 cm^{-1} experimental band.

If we now move to multiply bonded cases, the inclusion of a Mn atom in the bridge site lowers the stretching

TABLE 5

Calculated and Experimental NO Stretching Frequencies on Pd_3Mn Model Surfaces at 0.25-ML Coverage

Surface:	(100)							(111)				
Site:	Top Pd	Top Pd tilted	Top Mn	Bridge Pd–Mn	Pseudo threefold Pd_2–Mn		Lying down	Top Pd tilted	Top Mn	Bridge Pd–Pd	Hollow Pd_2–Mn	Hollow Pd_3
Label	A	B	C	D	E		F	G	H	I	J	K
ν (cm^{-1})	1738	1684	1688	1540	1421		992	1688	1690	1600	1460	1544
Experimental ν (cm^{-1})				1730	1695	1640	1560	1540	1510	1455		

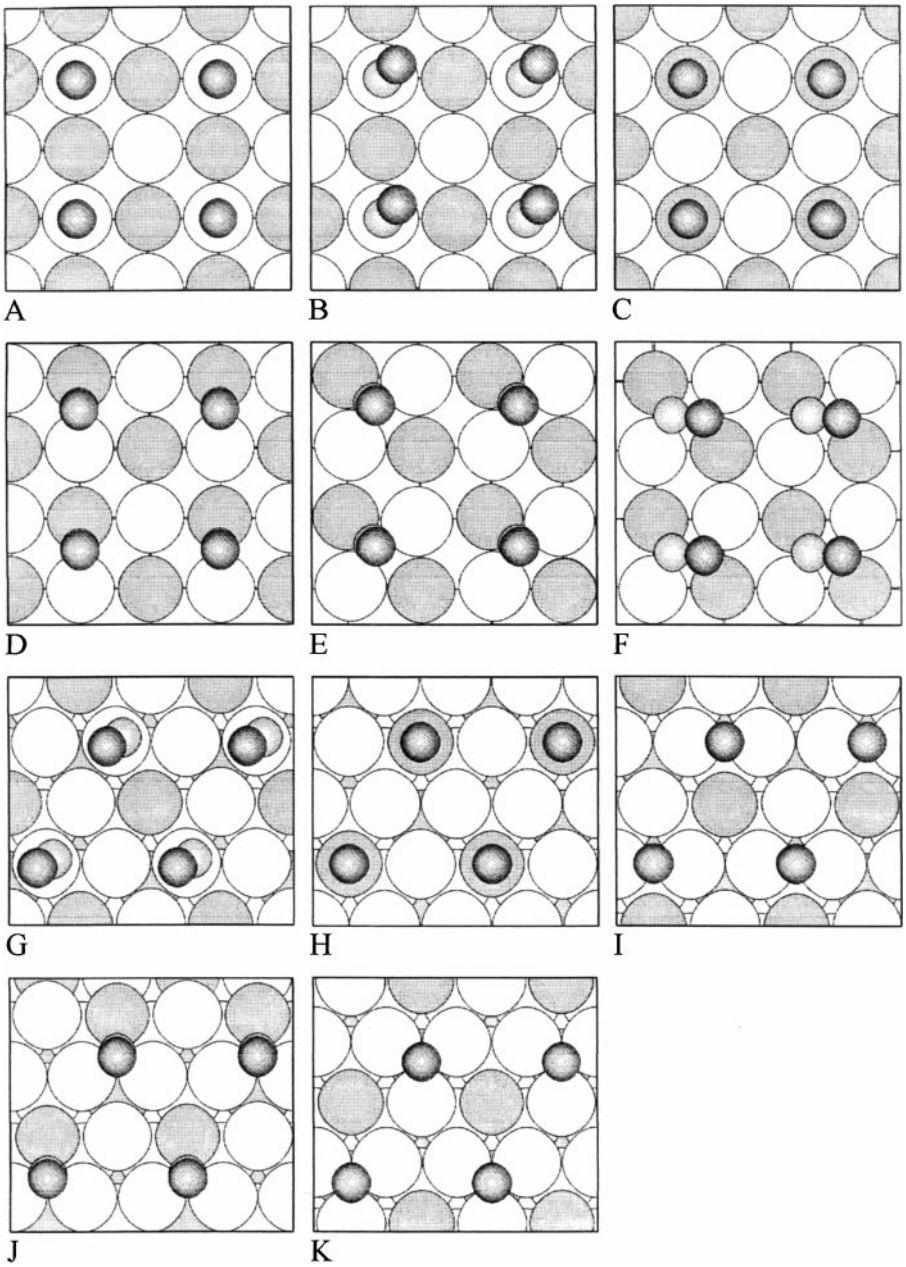

FIG. 9. Schematics of the structures considered for the calculation of the NO stretching frequency on Pd_3Mn (100) and (111) surfaces. In these top views, the O (respectively N) atom of the molecule is seen as a small dark (respectively light) ball, the Pd atom as a large white ball, and the Mn atom as a large gray ball. Labels are identical to those of Table 5: (A–E) top vertical on Pd, top tilted on Pd, top on Mn, bridge and pseudo threefold sites at 0.25-ML coverage on Pd_3Mn (100); (F) lying down structure on Pd_3Mn (100); (G–K) top on Pd, top on Mn, bridge and hollow sites at 0.25-ML coverage on Pd_3Mn(111).

frequency of this site on the (100) surface to 1540 cm^{-1}, hence the assignment of the 1640 cm^{-1} broad peak becomes more problematic on the alloy. Note that this band is broad and seems to be composed of a large number of subbands. The Pd–Pd bridge site on the (111) model alloy surface shows a much smaller shift with a frequency of 1600 cm^{-1} and it can be projected that Pd–Pd sites further away from Mn atoms will present a NO frequency closer to the pure Pd surface case. So, the left end of the band at 1640 cm^{-1} may be attributed to Pd–Pd bridge site adsorption on Pd-rich area, while the right end around 1610 cm^{-1} could be assigned to Pd–Pd sites in direct contact with a Mn atom, with all the possible intermediate situations inbetween. For the threefold sites, the frequency shift also depends on the number of Mn atoms in the triangle. The Pd_3 site of structure K shows a shift to lower frequency of 30 cm^{-1}, compared with pure Pd, while Pd_2Mn sites show a much larger effect with shifts of 80–110 cm^{-1}. This explains the large number of peaks in the spectrum in the low-frequency zone: the band at 1455 cm^{-1} can be attributed to Pd_2Mn mixed hollow sites, while the Pd_3 hollow sites and the Pd–Mn bridge site contribute to the multiple band between 1510 and 1560 cm^{-1}. It should be noted here that the ordered models for the alloy calculations impose a restricted number of site configurations, compared with the actual alloy surface which should present a richer spectrum.

Very important additional information from the calculations is that on the (100) alloy surface the NO molecule can adopt a very stable lying down geometry, with an activated N–O bond (structure F). The corresponding low frequency (992 cm^{-1}), however, is out of the experimental measurement range. The long N–O bond (1.33 Å) and the very low frequency suggest that this structure is a precursor for dissociation. Such an elongated lying down NO structure does not exist on the Pd surface but has been proposed from an IR experiment of NO adsorption on Rh(100) (23). All the assignments resulting from the DFT calculations are presented in Table 5 and Fig. 10.

3.2.2. CO–NO coadsorption. Sequential CO–NO adsorptions have also been performed at 300 K, each adsorption being followed by an evacuation for 30 min at 300 K, before recording the spectrum. Figure 11 shows this sequence performed on pure Pd. The spectrum represented by the solid line, identical to that in Fig. 5, is obtained after CO adsorption; if now NO is chemisorbed on this surface, one notes (dashed line) that the spectrum is similar of that in Fig. 6, obtained by adsorption of this molecule on the bare Pd surface. Similarly, the NO–CO sequence (doted line) leads again to the spectrum of pure CO. So, as a rough guess, each gas displaces the other, implying that these molecules are adsorbed on the same sites. However, the intensities of the CO IR bands, especially that of the linear form at 2080 cm^{-1}, are reduced after the NO adsorption, probably because partial coverage of the surface by strongly

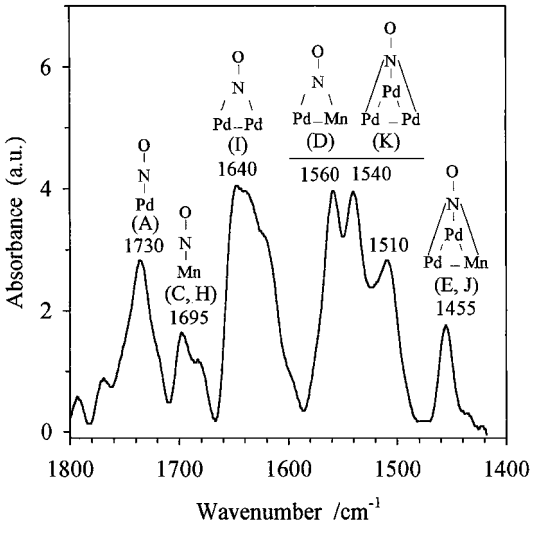

FIG. 10. Assignment of the IR bands of NO adsorbed on $P_{65}Mn_{35}$ from theoretical calculations.

adsorbed NO species has occurred. This phenomenon has already been observed by Oh and Carpenter (24). Calculations show that on a Pd(111) surface the binding energy of NO is 0.1–0.3 eV higher than that of CO, depending on the coverage. This is well in line with the observation of an almost complete displacement of CO by NO, but only a partial displacement of NO by CO.

The sequential adsorptions performed on the $Pd_{65}Mn_{35}$ catalyst are presented in Fig. 12, which shows that after the CO–NO sequence, the band assigned to hollow bonded CO (1860 cm^{-1}) is strongly reduced (dashed line). The band near 1650 cm^{-1} is not significantly modified. It has two possible assignments, CO in fourfold mixed sites or NO in bridge Pd_2 sites, so that a clear-cut conclusion is difficult. The last

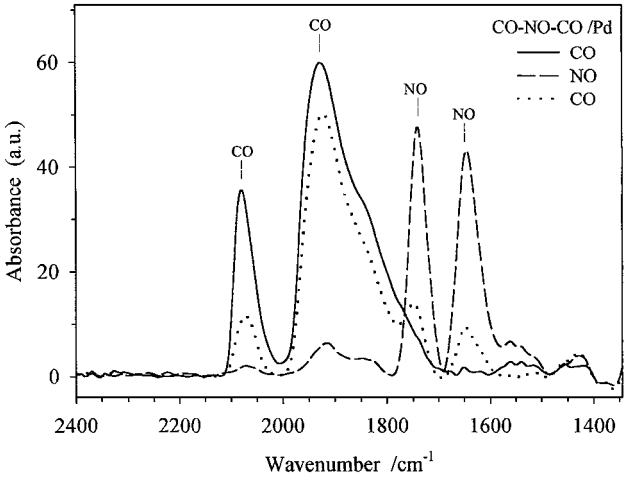

FIG. 11. Sequential CO–NO adsorption at 300 K on Pd/SiO_2: CO, solid line, then NO, dashed line, then CO, dotted line.

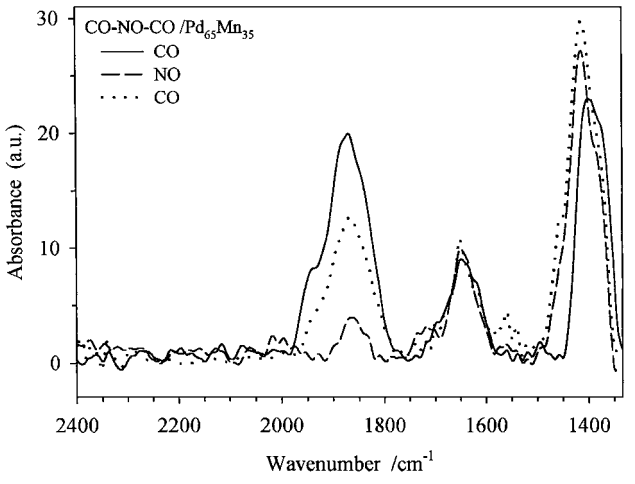

FIG. 12. Sequential CO–NO adsorption at 300 K on $Pd_{65}Mn_{35}$ catalyst: CO, solid line, then NO, dashed line, then CO, dotted line.

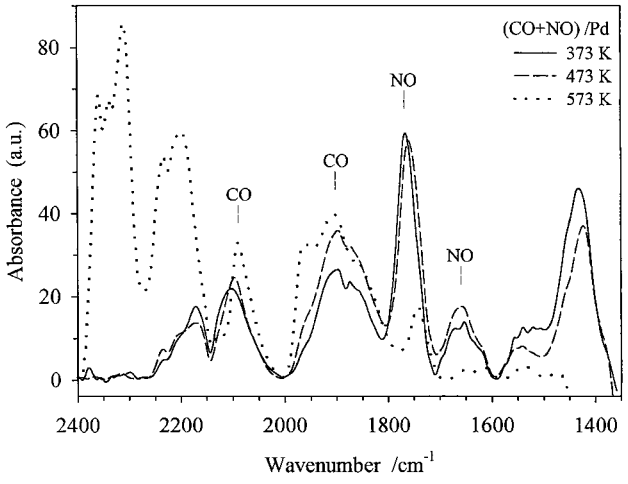

FIG. 13. Coadsorption of an equimolecular CO–NO mixture on Pd/SiO_2 at 373 K (solid line), 473 K (dashed line), and 573 K (dotted line).

CO band is located at 1400 cm^{-1}. It can be assigned to carbonates and carboxylates (1410–1420 cm^{-1}), $MnCO_2$ (see Fig. 5), and its intensity remains unchanged after NO consecutive adsorption. On NO introduction, a new and intense band appears at 1415 cm^{-1}, corresponding to NO in mixed Pd_2Mn sites. Our conclusion is that CO is to a large extent displaced by NO.

The final adsorption of CO modifies only moderately the spectrum: the NO in mixed Pd_2Mn sites (1415 cm^{-1}) are still present and the CO band at 1860 cm^{-1} is only partially rebuilt. This is in good agreement with calculated bonding energies. As is already the case on Pd, the chemisorption of NO is favored over that of CO on the alloy. However, the energy difference between the two molecules is increased to 0.6–0.7 eV in the alloy (25). Therefore, on PdMn, the competition for chemisorption tends to favor NO.

3.2.3. CO–NO coadsorption at higher temperature. The preceding results have shown that new Pd–Mn adsorption sites play a role in the adsorption and coadsorption of the reagents at room temperature. Their influence has also been studied in the case of CO–NO coadsorptions at temperatures where NO reduction by CO occurs (6). IR spectra obtained after a coadsorption of 1.3 kPa of an equimolecular mixture of the two gases on Pd/SiO_2 at 373, 473, and 573 K, recorded without evacuation of the gas phase, are presented in Fig. 13. The bands of gaseous NO and CO expected respectively near 1900 and 2140 cm^{-1} are not observed. Those corresponding to chemisorbed CO have an intensity increasing with temperature, whereas those assigned to chemisorbed NO strongly decrease at 573 K. New features are observed at high wavenumbers: two large bands appear between 2160 and 2400 cm^{-1}. The lower-frequency bands (2150–2250 cm^{-1}) have been assigned to isocyanate species on metal (26), such as Pd–NCO at 2200 cm^{-1} and N_2O in the gas phase (2220 cm^{-1}). Those observed between 2300 and 2400 cm^{-1} correspond to Si–NCO (2300 cm^{-1}) (27) and to gaseous CO_2 (2350–2370 cm^{-1}).

They can be compared with the spectra shown in Fig. 14 recorded under the same conditions on $Pd_{65}Mn_{35}/SiO_2$. Despite the fact that these spectra are recorded without evacuation, the IR bands of gaseous NO and CO are also not observed. Also, the bands assigned to adsorbed NO species have reduced intensity compared with those of adsorbed CO. The two large bands located between 2160 and 2400 cm^{-1} have greatly increased intensity on $Pd_{65}Mn_{35}/SiO_2$ compared with Pd/SiO_2. Undoubtedly, in the presence of Mn, the adsorbed NO molecule has been reacting above 500 K, leading to the formation of isocyanates, CO_2, and N_2O.

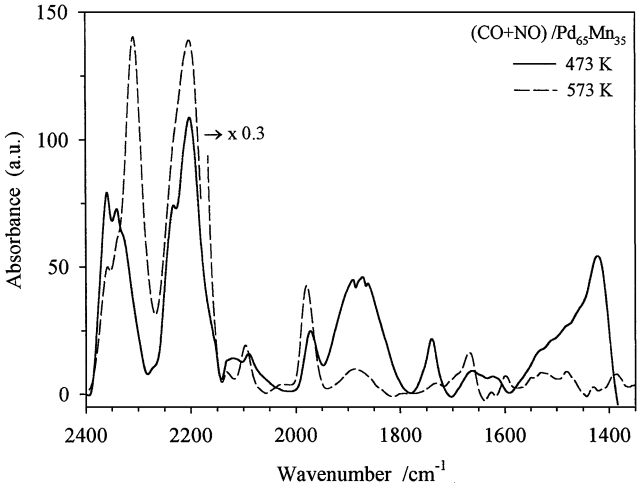

FIG. 14. Coadsorption of an equimolecular CO–NO mixture on the $Pd_{65}Mn_{35}$ catalyst at 473 K (solid line) and 573 K (dashed line) (between 2180 and 2400 cm^{-1}, the absorbance is multiplied by 0.3).

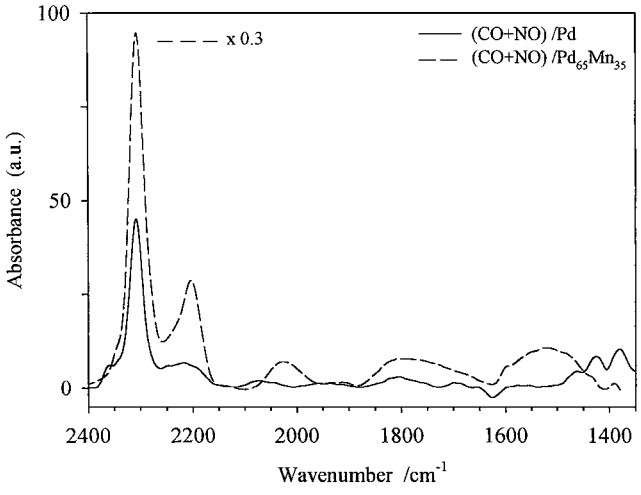

FIG. 15. Spectra observed on Pd/SiO_2 (solid line) and $Pd_{65}Mn_{35}$ (dashed line) (the absorbance is multiplied by 0.3) catalysts after adsorption of an equimolecular CO–NO mixture at 573 K and evacuation at 573 K.

After evacuation of the gas phase at 573 K, the IR spectra are changed (Fig. 15). The bands at lower wavenumbers are drastically decreased: N_2O has been evacuated. In the same way, the disappearance of the band at 2350–2370 cm^{-1} is explained by the evacuation of CO_2. The bands corresponding to isocyanates are stable and much more intense on the alloy than on pure palladium.

Therefore, the presence of Mn, which increases the dissociative adsorption of NO, leads to a reaction pathway such as NO_{ads} or $CO_{ads} + N_{ads} \rightarrow N_2O$ or –NCO.

4. DISCUSSION

According to the results on the NO–CO reaction mechanism reported in the literature, the NO dissociative adsorption is generally considered as the rate-determining step (27). The IR experiments reported above show that it is favored by the presence of Mn in the bimetallic particles or on the support. To justify the choice of the Pd_3Mn surface on which the DFT calculations are based, let us discuss the experimental results on surface composition.

4.1. Surface Composition

As mentioned above, the LEIS data represented in Fig. 3 indicate that marked segregation of Mn occurs at the surface. There may, however, be difficulty with respect to the reliability of the measured concentration ratios, because of the presence of manganese oxide on the support. Its amount, obtained by comparison of the chemical analysis and EDX experiments performed on the particles (8), is approximately 30%. But as shown in Fig. 4, its contribution to the overall Mn signal can be neglected. Indeed, similar conclusions were drawn by Jacobs *et al.* (28) from their comparative study of metals and oxides. They found that the LEIS signal of nickel in NiO is only respectively 10 and 20% of the values found for $Ni_{80}Pt_{20}$ and Ni–Al alloys.

Finally, with the figures given above, one can conclude that the Pd concentration at the surface of the $Pd_{65}Mn_{35}$ particles is on the order of 35 ± 10 at.%, with a large uncertainty resulting from the poor accuracy of the Mn sensitivity factor.

Thus, if the migration of Mn to the surface of the catalysts is established, accounting for the difference between surface and bulk compositions, this segregation concerns only one or two layers, since after 3 min of analysis, the measured Mn concentration is already reduced by one-half.

Even if there is some reservation on the LEIS results, the conclusions of the modeling carried out on the basis of "the equivalent-medium approximation" confirm the large segregation of the manganese at the surface. This method, described in (29), has already been applied successfully to the Pd–(Fe, Ni, Cu) single-crystal surfaces, leading to total agreement with the LEIS results on these well-defined systems. It was also applied by "a Monte-Carlo procedure" to 3-nm Pd–Pt clusters (30) produced by laser vaporization of bulk alloys and deposited on flat graphite surfaces; in that case, the agreement with the ion scattering experiments was again excellent.

Briefly, the input data for the simulation are the pair interaction energies of atoms in different binding sites, i.e., site energies in clusters of truncated cubo-octahedral shape. These data are taken from Ref. (30) for palladium atoms and derived from the model proposed by Donnely and King (31) for manganese atoms. The interaction potentials between uneven atoms are determined by assuming that Pd–Mn alloy is a substitution solid solution, with the same heat of mixing as the $Pd_{50}Mn_{50}$ alloy reported in Ref. (32).

Our calculations take into account the size of the clusters, but are limited, for practical reasons, to a diameter of 4 nm (2406 atoms); they are based on the particle composition measured by EDX and performed for an equilibration temperature of 600 K. One can observe in Table 1 that the predictions of surface composition do conclude to a marked segregation of Mn, although less important than that measured by LEIS. One should remark that the structure of a Pd_3Mn alloy (100) face (33) has been studied by low-energy electron diffraction; it has been concluded that the top layer forms a checkerboard, with a 50–50 composition and a $c(2 \times 2)$ ordered structure. This is in agreement with what is found on the aggregates.

Another important feature, which comes out of the modeling, is that the Mn atoms segregate on low coordination sites. Thus, the consequence is a decrease in the number of corner and edge sites occupied by Pd atoms, the preferential sites for apical adsorption, and explains the weakening on the alloys of the band assigned to linear CO.

Table 1 presents the results of analytical microscopy and EXAFS of Ref. (8), of the modeling, and of LEIS. The determination of composition performed by EDX has shown that all observable particles do contain a small proportion of manganese, 5% for the $Pd_{90}Mn_{10}$ catalyst and 25% for the $Pd_{65}Mn_{35}$ sample. Both the Monte-Carlo and LEIS results indicate that the top layer of the particles contains more manganese than the mean value measured by EDX. All these results on the study of surface composition constitute a justification for performing DFT calculations on an ordered $Pd_{75}Mn_{25}$ alloy.

Two reasons can be invoked to explain the improvement of NO reduction in the presence of manganese: either the specific catalytic behavior of electronically modified Pd sites or a peculiar role played by MnO_x species on the support. We are going to consider successively these two possibilities.

4.2. *Modifications of the Electronic Structure of Palladium by Alloying*

Let us consider the first possibility, i.e., an effect of Pd–Mn dual sites and/or a modification of the electronic structure of Pd by its Mn neighbors.

One should first note that our attempts to detect experimentally by XPS an effect of Mn atoms on the electronic structure of Pd were not successful. The Pd $3d_{5/2}$ core level is located at the same energy as for the reference sample, i.e., 335.2–335.5 eV, whatever the treatment to which the solid has been submitted in the preparation chamber. This can be ascribed to several factors. First, only 13 at.% manganese is alloyed to Pd in the $Pd_{65}Mn_{35}$ catalyst. Additionally, the expected shift is only 0.4–0.6 eV, the same order of magnitude as the resolution of the spectrometer, 0.3 eV.

It should, however, be mentioned that recently, Largentière *et al.* (34), in a study on the same system, but supported on alumina, did conclude an electronic effect, namely, a charge transfer from Pd to Mn. However, the procedure employed by these authors to introduce the catalysts into the spectrometer is doubtful, because a preparation chamber was not available and they had to protect the surface with a hydrocarbon film. Moreover, these authors studied only the Pd $3d_{5/2}$ level, which showed an increase in binding energy of 0.6 eV.

Actually, comparative extended Hückel theory (EHT) calculations have been carried out to determine the energies of adsorption of CO and NO on (111) and (100) single-crystal faces of Pd and a Pd_3Mn alloy (35). It was found that a charge transfer from Mn to Pd occurs in the alloy, resulting in increased electron density on the surface Pd atoms, the Fermi level being pushed to higher energy by 0.6 eV. This is actually consistent with the conclusions of our experiments mentioned above. Indeed, the slight decrease in the population of the Pd *d* orbitals, which is predicted, is accompanied by an increased density of states in the *s* orbital: the overall balance is actually an increase in charge on palladium. Even if the EHT method is known to provide less accurate values for the energies than *ab initio* methods, the general tendency is certainly correct.

This has been confirmed very recently (25, 36, 37) by DFT calculations on Pd_3Mn(100) and (111) faces. The electronic structure of Pd atoms has been shown to be a function of their local environment. Indeed, on the models of the faces, two types of situations can occur. The surface Pd nearest neighbors can be only Pd atoms: in this case they bear an excess of 0.07 electron; however, in the second configuration, where 4 Mn atoms are surface nearest neighbors of Pd, this excess of charge is 0.23 e^-. So the charge transfer is marked for Pd atoms which are the first neighbors of a Mn atom, but rapidly disappears when moving away from the Mn atom.

The lowering of the stretching frequency of CO and NO on a mixed Pd–Mn site compared with pure Pd can be explained by increased filling of the molecule π^* orbitals for the alloy (37, 38). However, the increased charge on Pd atoms close to Mn is not the reason. A Mn atom in the site plays the main role in this frequency lowering, since an empty part of the *d* band is centered on this atom. For both CO and NO, the interaction between the molecule π^* orbitals and this vacant part of the *d* band is strong, yielding an in-phase combination positioned far below the Fermi level. This result is a fractional filling of the molecule π^* orbital. This effect is strong when a Mn atom is involved in the site, because of the good energy match between these empty *d* states on Mn and the molecule π^* orbitals. In the case of structure K in Fig. 9, all Pd atoms have Mn first neighbors and despite this fact the shift in ν_{NO} compared with the pure Pd case is only 30 cm^{-1}. The direct influence of Mn is hence the key point. This electronic effect is a first-order phenomenon. Clearly, additional influence will arise, especially from the vibrational coupling between the CO and NO adsorbates. This point is of course fully taken into account in the calculations, but it should be of similar amplitude on Pd and the alloys.

The consequences of this modification of the electronic structure of Pd is a decrease in the binding energies of both molecules adsorbed on the alloy compared with pure metal, inducing a decrease in the surface coverage by chemisorbed molecules. This might account for the large decrease in absorbance observed on the infrared spectra of both CO and NO adsorbed on the alloys as shown in Figs. 5 and 6. Besides these interpretations of the IR spectra, the DFT calculations are now able to determine the reaction pathways. The activation barriers for the NO dissociation on different faces of palladium and Pd_3Mn can thus be compared.

Actually, the problem is rather complex, since the NO molecule can be initially adsorbed on several different sites, which would lead to different pathways. The different possibilities have been considered and the corresponding

energies compared. This work will be presented elsewhere. The calculations show that on Pd, NO dissociation is associated with a large barrier of 1.9 eV, while on Pd_3Mn the barrier is reduced to 1 eV (39). The inclined and lying down NO structures mentioned above are precursor states for the dissociation on the alloy.

4.3. Role of MnO_x on the Support

Returning to the beginning of this discussion, one should now consider a possible role played by MnO_x entities dispersed on the silica support. Indeed, the presence of "labile oxygen" on MnO_x is ascertained by the formation of CO_2 observed in the gas phase after CO adsorption. This oxidation of CO by labile oxygen atoms would result in the formation of vacancies on the Mn oxide. This phenomenon was indeed postulated in the case of Pd, Pt deposited on ZrO_2 and CeO_2 (39). Therefore, a dual-functional mechanism involving both metallic Pd–Mn sites on which NO is adsorbed in a predissociation state and these oxygen vacancies of MnO_x can be invoked (40). Finally the NO reduction would occur according to the scheme

$$M_S\text{—N–O--}\square\text{–Mn–O} \Rightarrow M_S\text{–}N_{ads} + \text{O–Mn–O}$$

($\square$ = oxygen vacancy, M_S = metallic site).

5. CONCLUSION

The Pd–Mn catalysts constitute a complex system but with the help of modern techniques, a description of the catalytic sites has been obtained. The bimetallic particles composed of a palladium-rich alloy have a surface enriched in manganese, with manganese oxide on the support. The complex IR spectra observed on adsorption and coadsorption of the two molecules are explained perfectly by the DFT calculations. They show that the assignment of a given IR band is never straightforward: even those that have the same frequency on pure Pd and on the alloys can actually correspond to different adsorption sites. The main feature that emerge from this study is the lowering of the NO stretch frequencies by $\approx$100 cm^{-1} on the alloys, compared with pure Pd. This is well explained by a partial filling of the π^* orbital of the molecule on the Pd–Mn mixed sites. Also, the DFT calculations have definitively contributed to the understanding of the reactivity of the alloys: evidence of activated NO molecules, with long N–O bonds, precursors of the dissociation, has been obtained on (100) faces of the alloy. This would perfectly explain the lower temperature of conversion of CO by NO observed on Pd–Mn bimetallic catalysts compared with pure palladium.

Second, the MnO_x species, also present at the surface, can act as a mobile oxygen reservoir, regulating the amount of oxygen available both for the oxidation of CO and to incorporate oxygen atoms produced by the dissociation of NO. Hence, this association of palladium with an electron-donating element like Mn or Cr, but also perhaps V or Ti, has a strong promoting effect in this reaction.

REFERENCES

1. Herzog, P. L., *in* "Fourth International Congress on Catalysis and Automotive Pollution Control, CAPOC4, Brussels, 1997" (N. Kruse, A. Frennet, and J.-M. Bastin, Eds.), Studies in Surface Science and Catalysis, Vol. 116, p. 35. Elsevier, Amsterdam, 1998.
2. Van Yperen, R., Lindner, D., Mussman, L., Lox, E. S., and Kreuzer, T., *in* "Fourth International Congress on Catalysis and Automotive Control, CAPOC4, Brussels, 1977" (N. Kruse, A. Frennet, and J.-M. Bastin, Eds.), Studies in Surface Science and Catalysis, Vol. 116, p. 51. Elsevier, Amsterdam, 1998.
3. Shelef, M., *Chem. Rev.* **95**, 209 (1995).
4. Iwamoto, M., Yashiro, H., Shundo, S., Yu-u, Y., and Mizumo, N., *Appl. Catal.* **69**, L15 (1991).
5. Mergler, Y. J., Hoebink, J., and Nieuvenhuys, B. E., *J. Catal.* **167**, 305 (1997).
6. Trillat, J. F., Massardier, J., Moraweck, B., Praliaud, H., and Renouprez, A. J., *J. Catal.* **167**, 103 (1997).
7. El Hamdaoui, A., Bergeret, G., Massardier, J., Primet, M., and Renouprez, A., *J. Catal.* **148**, 47 (1994).
8. Renouprez, A., Trillat, J. F., Moraweck, B., Massardier, J., and Bergeret, G., *J. Catal.* **179**, 390 (1998).
9. Niehus, P., Heiland, W., and Taglauer, E., *Surf. Sci. Rep.* **17**, 213 (1993).
10. Miegge, P., Rousset, J. L., Tardy, B., Massardier, J., and Bertolini, J. C., *J. Catal.* **149**, 143 (1994).
11. Renouprez, A. J., Lebas, K., Bergeret, G., Rousset, J. L., and Delichere, P., *in* "Proceedings of the 11th International Congress on Catalysis—40th Anniversary, Baltimore, 1996" (J. W. Hightower, W. N. Delgass, E. Iglesia, and A. T. Bell, Eds.), Studies in Surface Science and Catalysis, Vol. 101, p. 1105. Elsevier, Amsterdam, 1996.
12. Moulder, J. F., Sticle, W. F., Sobol, P. E., and Bonben, K. D., *in* "Handbook of X-Ray Photoelectron Spectroscopy" (J. Chastain, Ed.). Perkin–Elmer Corp., 1992.
13. Loffreda, D., Simon, D., and Sautet, P., *Surf. Sci.* **425**, 68 (1999).
14. Loffreda, D., Simon, D., and Sautet, P., *Chem. Phys. Lett.* **291**, 15 (1998).
15. Kresse, G., and Furthmuller, J., *Phys. Rev. B* **54**, 11169 (1996).
16. Perdrew, J. P., Chevary, J. A., Vosko, S. H., Jackson, K. A., Pederson, M. R., Singh, D. J., and Fiolhais, C., *Phys. Rev. B* **46**, 6671 (1992).
17. Hoffmann, F. M., and Bradshaw, A. M., *Surf. Sci.* **72**, 513 (1978).
18. Blyholder, G., and Allen, M. C., *J. Am. Chem. Soc.* **91**, 3158 (1969).
19. Kiselev, V. A., and Krilov, V. O., *in* "Adsorption and Catalysis on Transition Metals and Their Oxides," Vol. 9. Springer-Verlag, Berlin, 1989.
20. Srivinas, G., Wright, J., and Cook, R., *in* "Proceedings of the 11th International Congress on Catalysis—40th Anniversary, Baltimore, 1996" (J. W. Hightower, W. N. Delgass, E. Iglesia, and A. T. Bell, Eds.), Studies in Surface Science and Catalysis, Vol. 101, p. 427. Elsevier, Amsterdam, 1996.
21. Moriki, S., Inoue, Y., Miraki, E., and Yasumori, J., *J. Chem. Soc. Faraday Trans. 1* **78**, 171 (1982).
22. Hoost, T. E., Otto, K., and Laframboise, K. A., *J. Catal.* **155**, 303 (1995).
23. Villarubia, J. S., and Ho, W., *J. Chem. Phys.* **87**, 750 (1987).
24. Oh, S. H., and Carpenter, J. E., *J. Catal.* **101**, 114 (1986).
25. Delbecq, F., and Sautet, P., *Chem. Phys. Lett.* **302**, 91 (1999).
26. Paul, D. K., McKee, M. L., Worley, S. D., Hoffman, M. W., Ash, D. H., and Gautney, J., *J. Phys. Chem.* **93**, 4598 (1989).

27. Hecker, W. C., and Bell, A. T., *J. Catal.* **85**, 389 (1984).
28. Jacobs, J. P., Reijne, S., Elfrink, R. J. M., Mikhailov, S. N., and Brongersma, H. H., *J. Vac. Sci. Technol. A* **12**, 2308 (1994).
29. Rousset, J. L., Bertolini, J. C., and Miegge, P., *Phys. Rev. B* **53**, 4947 (1996).
30. Rousset, J. L., Renouprez, A. J., and Cadrot, A. M., *Phys. Rev. B* **58**, 2150 (1998).
31. Donnely, R. G., and King, T. S., *Surf. Sci.* **74**, 89 (1978).
32. De Boer, F. R., Boom, R., Mattens, W. C. M., Miedema, A. R., and Niessen, A. K., *in* "Cohesion in Metals. Transition Metal Alloys." North-Holland, Amsterdam, 1988.
33. Tian, D., Lin, R. F., Jona, F., and Marcus, P. M., *Solid State Commun.* **74**, 1017 (1990).
34. Largentière, P. C., Canon, G. C., and Figoli, N. S., *Appl. Surf. Sci.* **89**, 63 (1995).
35. Delbecq, F., Moraweck, B., and Vérité, L., *Surf. Sci.* **396**, 156 (1998).
36. Delbecq, F., and Sautet, P., *Phys. Rev. B* **59**, 5142 (1999).
37. Delbecq, F., and Sautet, P., *Surf. Sci.* **442**, 338 (1999).
38. Loffreda, D., Ph.D. thesis, Lyon, 1999.
39. Skoglundh, M., Torncrona, A., Thormahlen, P., Fridell, E., Drewsen, A., and Jobson, E., *in* Proceedings of the Fourth International Congress on "Catalysis and Automotive Pollution Control, CAPOC4, Brussels, 1997" (N. Kruse, A. Frennet, and J.-M. Bastin, Eds.), Studies in Surface Science and Catalysis, Vol. 116, p. 113. Elsevier, Amsterdam, 1998.
40. Baltanas, M. A., *Appl. Catal.* **2**, 15 (1986).